REPORT DOCUMENTATION PAGE

Form Approved
OMB No. 0704-0188

1. REPORT DATE *(DD-MM-YYYY)*
21-06-2005

REPRINT

4. TITLE AND SUBTITLE
Stormtime Subauroral Density Troughs: Ion-molecule Kinetics Effects

5a. CONTRACT NUMBER

5b. GRANT NUMBER

5c. PROGRAM ELEMENT NUMBER
61102F

6. AUTHOR(S)
E.V. Mishin*, W.J. Burke and A.A. Viggiano

5d. PROJECT NUMBER
2311

5e. TASK NUMBER
SD

5f. WORK UNIT NUMBER
A3

7. PERFORMING ORGANIZATION NAME(S) AND ADDRESS(ES)
Air Force Research Laboratory/VSBXP
29 Randolph Road
Hanscom AFB MA 01731-3010

8. PERFORMING ORGANIZATION REPORT NUMBER
AFRL-VS-HA-TR-2005-1073

9. SPONSORING / MONITORING AGENCY NAME(S) AND ADDRESS(ES)

10. SPONSOR/MONITOR'S ACRONYM(S)

11. SPONSOR/MONITOR'S REPORT NUMBER(S)

12. DISTRIBUTION / AVAILABILITY STATEMENT
Approved for Public Release; Distribution Unlimited.

*Boston College, Institute for Scientific Research, Chestnut Hill, MA

13. SUPPLEMENTARY NOTES
REPRINTED FROM: JOURNAL OF GEOPHYSICAL RESEARCH, Vol 109, A10301, doi: 10.1029/2004JA010438, 2004.

14. ABSTRACT

[1] We report on subauroral plasma density troughs observed by Defense Meteorological Satellite Program (DMSP) satellites during the major magnetic storm of 6 April 2000. The troughs were embedded within strongly irregular, ≥500-km wide subauroral convection streams, composed of two distinctive parts. The poleward part coincided with strong wave structures, energetic (ring current) ion precipitations, and enhanced vertical ion flows. One or several narrow density decreases were present here. The equatorward part was marked by a density trough coincident with a local maximum of the electron temperature ~7000–9000 K. Here the ion temperatures and downward vertical ion velocities were ~2000 K and <20 m/s, respectively. The mean convection velocity was typically ≤500 m/s. We develop analytical approximations for the rate coefficients of the charge exchange reactions based on recent laboratory experiments. These have been used in local modeling of the equatorward *F* peak density depletions. Topside steady-state density profiles were evaluated assuming diffusive equilibrium in a given T_e profile. A scenario for the transition of an initial density-height profile to a flat profile is described. Substantial agreement between the modeling results and DMSP observations indicates that the vibrational mechanism contributes significantly to the formation of high-T_e-related density troughs.

15. SUBJECT TERMS
Ionosphere/magnetosphere interactions Stormtime subauroral density troughs
Elevated electron temperature Vibrational excitation DMSP

16. SECURITY CLASSIFICATION OF:			17. LIMITATION OF ABSTRACT	18. NUMBER OF PAGES	19a. NAME OF RESPONSIBLE PERSON
a. REPORT		c. THIS PAGE			W. Burke
UNCLAS	UNCLAS	UNCLAS	SAR		19b. TELEPHONE NUMBER *(include area code)* 781-377-3980

Standard Form 298 (Rev. 8-98)

JOURNAL OF GEOPHYSICAL RESEARCH, VOL. 109, A10301, doi:10.1029/2004JA010438, 2004

Stormtime subauroral density troughs: Ion-molecule kinetics effects

E. V. Mishin
Institute for Scientific Research, Boston College, Chestnut Hill, Massachusetts, USA

W. J. Burke and A. A. Viggiano
Space Vehicles Directorate, Air Force Research Laboratory, Hanscom Air Force Base, Massachusetts, USA

Received 13 February 2004; revised 6 May 2004; accepted 28 July 2004; published 8 October 2004.

[1] We report on subauroral plasma density troughs observed by Defense Meteorological Satellite Program (DMSP) satellites during the major magnetic storm of 6 April 2000. The troughs were embedded within strongly irregular, $\geq$500-km wide subauroral convection streams, composed of two distinctive parts. The poleward part coincided with strong wave structures, energetic (ring current) ion precipitations, and enhanced vertical ion flows. One or several narrow density decreases were present here. The equatorward part was marked by a density trough coincident with a local maximum of the electron temperature ~7000–9000 K. Here the ion temperatures and downward vertical ion velocities were ~2000 K and <20 m/s, respectively. The mean convection velocity was typically $\leq$500 m/s. We develop analytical approximations for the rate coefficients of the charge exchange reactions based on recent laboratory experiments. These have been used in local modeling of the equatorward F peak density depletions. Topside steady-state density profiles were evaluated assuming diffusive equilibrium in a given T_e profile. A scenario for the transition of an initial density-height profile to a flat profile is described. Substantial agreement between the modeling results and DMSP observations indicates that the vibrational mechanism contributes significantly to the formation of high-T_e-related density troughs. *INDEX TERMS:* 2431 Ionosphere: Ionosphere/magnetosphere interactions (2736); 2435 Ionosphere: Ionospheric disturbances; 2467 Ionosphere: Plasma temperature and density; 2481 Ionosphere: Topside ionosphere; 2768 Magnetospheric Physics: Plasmasphere; *KEYWORDS:* stormtime subauroral density troughs, elevated electron temperatures, vibrational excitation

Citation: Mishin, E. V., W. J. Burke, and A. A. Viggiano (2004), Stormtime subauroral density troughs: Ion-molecule kinetics effects, *J. Geophys. Res.*, *109*, A10301, doi:10.1029/2004JA010438.

1. Introduction

[2] During magnetic substorms and storms, deep plasma density troughs form in the evening sector at subauroral latitudes in the topside ionosphere [e.g., *Spiro et al.*, 1979; *Evans et al.*, 1983; *Anderson et al.*, 1991, 1993]. These are often associated with enhanced streams of westward plasma convection, described by the names polarization jets (PJ) [*Galperin et al.*, 1974] or subauroral ion drifts (SAID) [*Spiro et al.*, 1979; *Anderson et al.*, 1991, 1993]. Recently, *Foster and Burke* [2002] suggested the name Subauroral Polarization Streams (SAPS) to include plasma flow events that have both broad and narrow extents in latitude. Stable Auroral Red (SAR) arcs are also observed within stormtime troughs. Their 630.0-nm emissions are caused by elevated electron temperatures, $T_e \gtrsim 3000$ K [e.g., *Newton et al.*, 1974; *Rees and Roble*, 1975; *Foster et al.*, 1994]. These are explained as consequences of heat conduction due to the ring current-plasmasphere interactions [e.g., *Kozyra et al.*, 1987; *Jordanova et al.*, 1999; *Liemohn et al.*, 2000].

0148-0227/04/2004JA010438$09.00

[3] The ion population of the topside F region below 1000 km is dominated by O^+. As their recombination rate is very small, ionization balance is mainly determined by rapid recombination of NO^+ and O_2^+, stemming from the ion-molecule reactions

$$\text{(R1)} \qquad O^+ + N_2 \xrightarrow{k_1} NO^+ + N$$

$$\text{(R2)} \qquad O^+ + O_2 \xrightarrow{k_2} O_2^+ + O$$

The rate coefficients k_1 and k_2 vary with the energies of interacting species. Experiments in drift tubes specified the dependences of k_1 and k_2 on the ion translational energy $\varepsilon_i \propto \mathbf{V_d^2}$ [e.g., *McFarland et al.*, 1973; *Albritton et al.*, 1977]. Here $\mathbf{V_d} = \mathbf{cE_0} \times \mathbf{B/B^2}$ and $\mathbf{E_0}$ is the electric field (c is the speed of light). On the other hand, it is known that k_1 and k_2 also increase with the level of the vibrational excitation of N_2 and O_2, respectively [*Schmeltekopf et al.*, 1967, 1968; *Hierl et al.*, 1997]. In thermal equilibrium the vibrational population is defined by a Boltzmann distribution with a vibrational temperature T_V.

[4] The coincidental formation of plasma density troughs and SAPS structures has been explained through a combination of enhanced recombination stemming mainly from the reactions (R1) and (R2) and plasma outflows due to frictional ion heating [*Newton and Walker*, 1975; *Schunk et al.*, 1975, 1976; *Banks and Yasuhara*, 1978; *Anderson et al.*, 1991; *Moffet et al.*, 1998; *Pavlov*, 1998; *Pavlov et al.*, 2000; *Pavlov and Foster*, 2001; *Vlasov and Kelley*, 2003]. We define the trough depth as $\delta n_m = (n_0 - n_{\min})/n_0$, where $n_{\min}$ (n_0) is the minimum (background) electron density. Note that $\delta n_m \rightarrow 1$ when $n_{\min} \rightarrow 0$.

[5] *Newton and Walker* [1975] and *Moffett et al.* [1998] found that making allowance for vibrational excitation of N_2 at $T_e \sim 3000-4000$ K reduced the electron density in the F region by a factor of $\lesssim 2$ (i.e., $\delta n_m \lesssim 0.5$). Using the updated rates, *Pavlov and Foster* [2001] showed that vibrational excitations at $T_e \sim 3000$ K lead to $\delta n_m \simeq 0.65$ in the daytime ionosphere at ~300–350 km. *Schunk et al.* [1975, 1976] showed that enhanced recombination caused by intense electric fields ≥ 0.1 V/m yields $\delta n_m \simeq 0.65-0.75$ at ≥ 300 km. Note that $E_0 \sim 0.1$ V/m corresponds to horizontal convection velocities $V_H = V_d \simeq 2$ km/s. In addition, *Schunk et al.* [1975] states that the presence of strong vibrationally excited N_2 with $T_V \simeq 4600$ K is equivalent to the effect of ~0.1 V/m electric fields. Overall, these investigations agree that the vibrational mechanism cannot solely account for the trough formation. *Anderson et al.* [1991] suggested that ion outflows with mean velocities ~500–800 m/s due to frictional ion heating are the main cause of deep troughs $\delta n_m \geq 0.75-0.9$.

[6] The commonly accepted scenario for SAPS-related troughs relies on plasma streams with large, typically $V_H \geq 2$ km/s, velocities and strongly elevated ion temperatures. Indeed, usually T_e enhancements are either less noticeable or at times $\sim T_i$. For example, *Moffet et al.* [1998] presented observations from the DE-2 satellite at altitudes ~456, 415, and 315 km of three troughs with $V_H \simeq 2.3$, 2, and 4 km/s and T_i (T_e) $\simeq 4000$ (3000), 4500 (4500), and 5000 (2500) K, respectively.

[7] However, *Förster et al.* [1999] and *Mishin et al.* [2003] reported observations of unusual subauroral troughs during the 21 March 1990 and 6 November 2001 magnetic storms. The first one, with $\delta n_m \simeq 0.67$ at ~700 km altitude and 56.6° magnetic latitude, was encountered in the dusk sector (at 18.5 MLT) during a nearby pass of the Active satellite above the Millstone Hill radar. The electron temperature increased to 7200 K within the trough, while the ion temperature remained ≤ 2000 K, comparable to that in the adjacent midlatitude region. Simultaneous observations from the Millstone Hill radar agreed with the satellite observations and showed that the density depletion and enhanced $T_e \simeq 3500$ K at ≥ 400 km altitude were embedded within a SAPS with $V_H \simeq 0.7-1$ km/s. The latter agreed well with measurements of $V_H \simeq 1.2$ km/s at ~830 km by the DMSP F8 satellite flying ~50 min earlier and later than the Active pass. *Förster et al.* [1999] also noted the presence of unusually high, $\sim 1.5 \times 10^2$ cm^{-3}, molecular ion densities within the trough at ~700 km.

[8] The 6 November 2001 SAPS event was observed by the DMSP F15 satellite at 0423 UT, after a sharp increase of the AE index from ~500 to ~2000 nT following a northward turning of IMF B_Z [*Mishin et al.*, 2003]. Within a $\delta n_m \simeq 0.75$ trough at ~830 km, T_e reached ≃9000 K, while $T_i \simeq 2000$ K, $V_H \simeq 0.5$ km/s, and a downward vertical flow velocity ≤ 20 m/s. Significantly, the density minimum occurred ~100 km equatorward of a strong SAPS wave structure. Here the term "strong" indicates that the peak to peak variability of V_H oscillations was of the same order or even exceeded the mean convection velocity $\langle V_H \rangle$. Enhanced fluxes of precipitating 30 keV ions, likely the low-energy portion of the ring current population, were collocated with the wave structure [*Mishin et al.*, 2003]. Apparently, this event reflected enhanced ring current-plasmasphere interactions, initiated by freshly injected particles [e.g., *Anderson et al.*, 1993; *Garner et al.*, 2004]. However, a special study is needed to determine how typical, with regards to the trough formation, these events are.

[9] The objectives of this paper are twofold. First, we report on the trough events associated with the strong SAPS wave structures during the 6 April 2000 magnetic storm (section 2). We found that all strong SAPS wave structures were accompanied by highly structured plasma density troughs. Typically, one of the density minima coincides with the wave structure, while another is displaced by ~100 km equatorward and coincides with the maximum of T_e. In section 3 we present analytical approximations for the rate coefficients of the reactions (R1) and (R2), derived from the latest experimental results [*Viggiano and Williams*, 2001]. These have been used in local modeling of the equatorward F peak density depletions, performed in section 4. To compare the modeling results with the DMSP observations, the topside density profiles above ~500 km were evaluated, assuming diffusive equilibrium in a given T_e profile, likewise *Schunk et al.* [1975, 1976].

2. Observations

2.1. Instrumentation

[10] DMSP satellites are three-axis stabilized spacecrafts that fly in circular, Sun-synchronous polar (inclination 98.7°) orbits at an altitude of ~840 km. The geographic local times of the orbits are either near the 1800–0600 (F13) or 2100–0900 (F12, 14, 15) meridians. Owing to the offset between the geographic and geomagnetic poles DMSP satellites sample wide range of magnetic local times (MLT) over the course of a day. The ascending nodes of DMSP orbits are on the duskside of the Earth. Thus the satellites move toward the northwest in the evening LT sector. Each satellite carries a suite of sensors to measure (1) fluxes of precipitating electrons and ions in the energy range between 30 eV and 30 keV (SSJ4); (2) the densities, temperatures, and drift motions of ionospheric ions and electrons (SSIES); and (3) perturbations of the Earth magnetic field (SSM). We do not use the SSM data in this study.

[11] SSJ4 sensors consist of four detectors, one high-energy (1–30 keV) detector and one low-energy (30–1000 eV) detector for each of the particle types [*Hardy et al.*, 1984]. Nineteen point ion and electron spectra are returned once per second. SSIES consists of (1) an ion drift meter to measure the horizontal (V_H) and vertical (V_V)

Table 1. The 6 April 2000 SAPS Wave Events

Sat Number	Event	UT	MLat	MLT
F11	11/23	2330	49°	1930
F12	12/23	2346	−45°	2042
F14	14/23	2307	−47°	2042
F15	15/22	2229	49°	2124
F15	15/23	2344	−46°	2118

cross-track components of plasma drift within the range of ±3000 m/s and a one-bit resolution of 12 m/s for ambient ion densities greater than $5 \times 10^3 cm^{-3}$; (2) a retarding potential analyzer to measure ion temperatures (T_i), composition, and the in-track component of plasma drift ($V_\parallel$); (3) an ion trap to measure the total ion density (n_i); and (4) a spherical Langmuir probe to measure the density (n_e) and temperature (T_e) of ambient electrons [*Rich and Hairston*, 1994]. The plasma drift and density measurements are sampled at the rates of 6 and 24 Hz, respectively, while T_e and T_i were sampled at a rate of 0.25 Hz.

2.2. SAPS Wave Events on 6 April 2000

[12] The main phase of the 6 April 2000 magnetic superstorm began at ~1650 UT and reached maximum epoch at ~2400 UT [e.g., *Huang and Burke*, 2004]. Throughout the main phase, a few short-lived magnetospheric disturbances occurred at ~2100, 2200, 2300, and 2320 UT. After 2200 UT, several strong SAPS wave structure events were observed in the evening sector by four DMSP satellites. Table 1 lists the universal times, magnetic latitude (MLat), and magnetic local times (MLT) of the observed structures. In general, all of these events resemble the 6 November 2001 event [*Mishin et al.*, 2003] (hereafter designated as Nov6). We consider strong wave structures as the benchmark for enhanced ring current-plasmasphere interactions, initiated by magnetic activity.

[13] Figure 1 provides an example typical of strong SAPS wave events. It was crossed by the DMSP F14 satellite at ~2306:30 to ~2308 UT (hereafter event 14/23) during a southern hemisphere pass in the evening sector at ~2042 MLT. The top two panels show directional differential number fluxes of downcoming electrons and ions, respectively. Horizontal (positive sunward) and vertical (positive upward) components of the convection velocity are shown in the third and fourth panels, respectively. The fifth panel shows variations of the electron and ion temperatures sampled with 4-s time resolution. Here dots and asterisks or diamonds and triangles designate the data obtained from the Air Force Research Laboratory (AFRL) [e.g., *Rich et al.*, 2003] or from the DMSP SSIES data distribution website (available at http://cindispace.utdallas.edu/DMSP/) at the University of Texas at Dallas (UTD). The bottom panel shows 1-s average values of the ion density.

[14] Attention is directed to the following four features of the data. (1) Significant fluxes of precipitating 1–30 keV ions were detected coincident with the strong wave structure. These fluxes probably represent the low-energy portion of the ring current distribution function [*Smith and Hoffman*, 1974]. (2) Fluxes of ~30–100 eV ions increased up to $\gtrsim 3 \times 10^5$ cm^{-2} s^{-1} $ster^{-1}$ eV^{-1} within the wave structure and disappeared at ~2307:30 UT. The flux of suprathermal (≤100 eV) electrons increased slightly to $\sim 3 \times 10^4$ cm^{-2} s^{-1} $ster^{-1}$ eV^{-1} within the wave structure. (3) Electron and ion temperatures were irregular within the region. Apparently, there is good agreement between the AFRL and UTD values for T_e. On the average, T_e increased within the wave structure up to ~8000 K, descended to a local minimum ~5200 K at ~2307:35 UT, increased again to a local maximum ~7500 K at ~2307:50 UT, and then gradually decreased. T_i values calculated with the AFRL and UTD algorithms show significant difference in the regions of energetic ion precipitation within, and poleward of, the wave structure. The difference is less than 20% after ~2307:30 UT. (4) The plasma density had two distinct minima, $\sim 3 \times 10^4$ cm^{-3}, near 2306:30 and 2307:35 UT, respectively. The former coincided with an increase in the energy and intensity of precipitating ions simultaneous with enhanced vertical ion flows ~±500 m/s. The second trough was detected after ~2307:05 UT, ≃1.8° equatorward of the wave structure. The density decreased gradually as did the energy of suprathermal ions and T_e, regardless of the varying ion temperature. At 2307:30 UT, n_i dropped by a factor of ~2 at the equatorial edge of the ion flux. At this time, the vertical component of the ion flow was downward ~20–40 m/s. After reaching the second minimum, n_i slightly increased and then decreased again to $\sim 4\ 10^4$ cm^{-3} at ~2307:45 UT. It steadily increased afterward. During this period the ion temperature, mean convection velocity, and downward vertical flow velocity remained ~2000 K, ≤400 m/s, and ~10 m/s, respectively.

[15] Similar behaviors characterized all of the equatorward trough events studied during the April 2000 storm. However, sometimes within the wave structure multiple, latitudinally narrow density decreases were present. To study effects of electron and ion heating, we only consider data acquired equatorward of the wave structures. Otherwise, the contribution of precipitating energetic ions and vertical plasma flows must be accounted for.

2.3. Plasma Density Variations

[16] Let us consider how relative plasma densities $\delta n_i/n_0 \equiv \delta n_i = (n_0 - n_i)/n_0$ vary with the mean (O^+) ion energy, $\varepsilon_{i-n}^{(1,2)}$, in the center of mass system of interacting species, that is O^+ and N_2 (or O_2)

$$\varepsilon_{i-n}^{(1,2)} = \frac{1}{2}\frac{m_i m_{1,2}}{m_i + m_{1,2}}\overline{(\mathbf{v_i} - \mathbf{v_{1,2}})^2} = \frac{3}{2}\frac{m_i m_{1,2}}{m_i + m_{1,2}}\left(\frac{T_i}{m_i} + \frac{T_{1,2}}{m_{1,2}} + \frac{m_i V_d^2}{3\kappa}\right). \quad (3)$$

Here n_0 stands for the plasma density at the equatorward edge of the SAPS, $\mathbf{V_d} = c\mathbf{E_0} \times \mathbf{B}/\mathbf{B}^2$, κ is the Boltzmann constant, and $\overline{()}$ designates average values over the Maxwell-Boltzmann ion and neutral distributions. Indices 1 and 2 stand for N_2 and O_2, respectively. As usual, the effective ion temperature is defined as $T_i^{(1,2)} = \frac{2}{3}\varepsilon_{i-n}^{(1,2)}$. To simplify calculations, we take $m_1 \simeq m_2 \simeq 2m_i$ and translational temperatures $T_1 = T_2 = T_n = 1000$ K, yielding $\varepsilon_{i-n}^{(1)} = \varepsilon_{i-n}^{(2)} = \varepsilon_{i-n}$ and $T_i^{(1)} = T_i^{(2)} = T_{in}$ [cf. *St.-Maurice and Torr*, 1978].

[17] By definition, $\widetilde{\delta n_i}$ increases as n_i decreases ($\widetilde{\delta n_i} \to \widetilde{\delta n_m}$ at $n_i \to n_{\min}$). If the ion translational energy controlled the

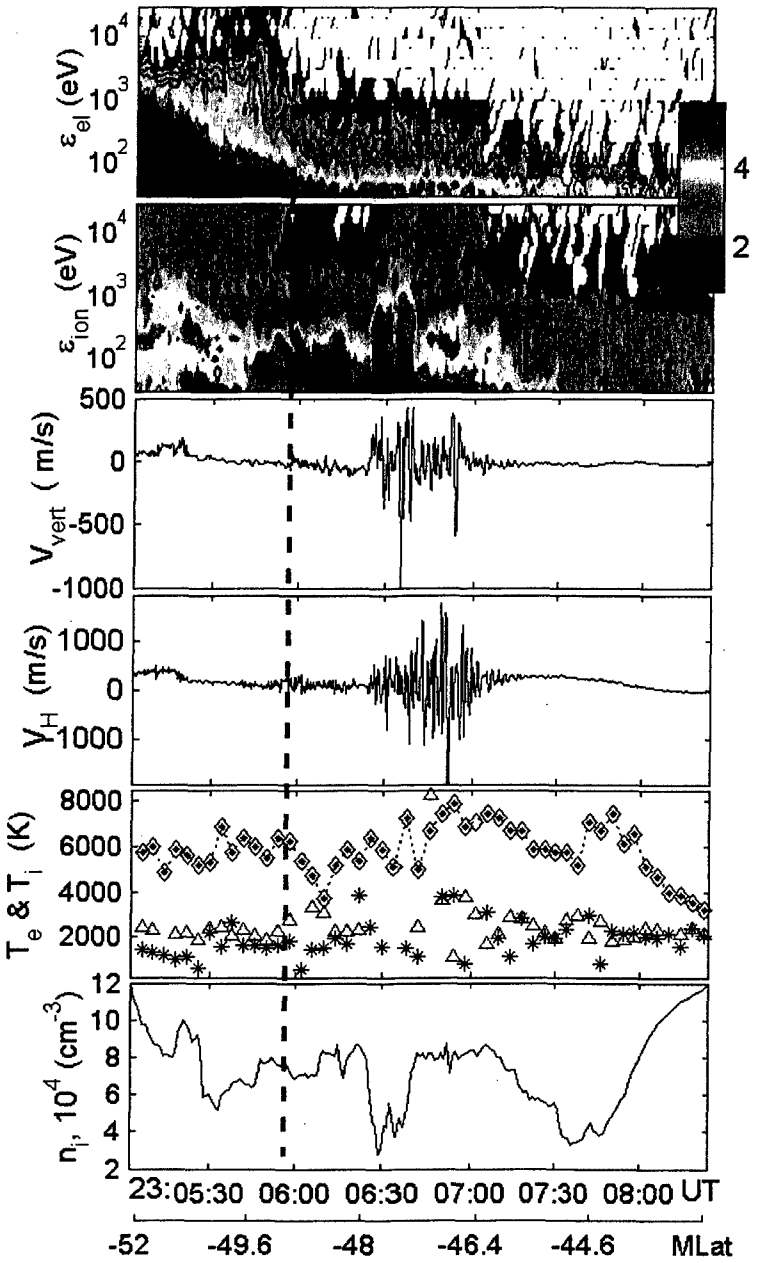

Figure 1. Example of SAPS wave structure observed by DMSP F14 at ~2307 UT on 6 April 2000 (event 14/23). Top panels show electron and ion energy-time spectrograms of downcoming directional differential number fluxes in $cm^{-2}\ s^{-1}\ ster^{-1}\ eV^{-1}$ (logarithmic scale). The third and fourth panels show vertical and horizontal components of the convection velocity, respectively. The fifth panel shows variations of the electron (dots and open diamonds) and ion (asterisks and open triangles) temperatures, as calculated using AFRL and UTD algorithms. The bottom panel shows 1-s averaged ion densities. The vertical dashed line indicates the equatorward boundary of the electron plasma sheet.

plasma density, $\widetilde{\delta n_i}$ should increase with ε_{i-n} [cf. *Schunk et al.*, 1975, 1976]. Figure 2a shows $\widetilde{\delta n_i}$ variations versus ε_{i-n} for the 12/23, Nov6, 14/23, 15/22, and 15/23 events (data gaps were present during the event 11/23). In general, $\widetilde{\delta n_i}$ appears to be independent of ε_{i-n} in all events save perhaps that of 12/23. The latter is the only event where the convection velocity at the equatorward side rose to ~1000 m/s ($E_0 \sim 50$ mV/m), yielding $\varepsilon_{i-n} \geq 4500$ K (see note in section 3.1).

[18] Figure 2b shows $\widetilde{\delta n_i}$ variations plotted as functions of T_e. In general, the density increased ($\widetilde{\delta n_i} \rightarrow 0$) at the equatorward side of the trough in step with electron temperature decreases. A linear approximation yields $\widetilde{\delta n_i} \simeq \widetilde{\delta n_0} + \widetilde{a} \cdot 10^{-4} \cdot T_e$ for $T_e > 3000$ K, where

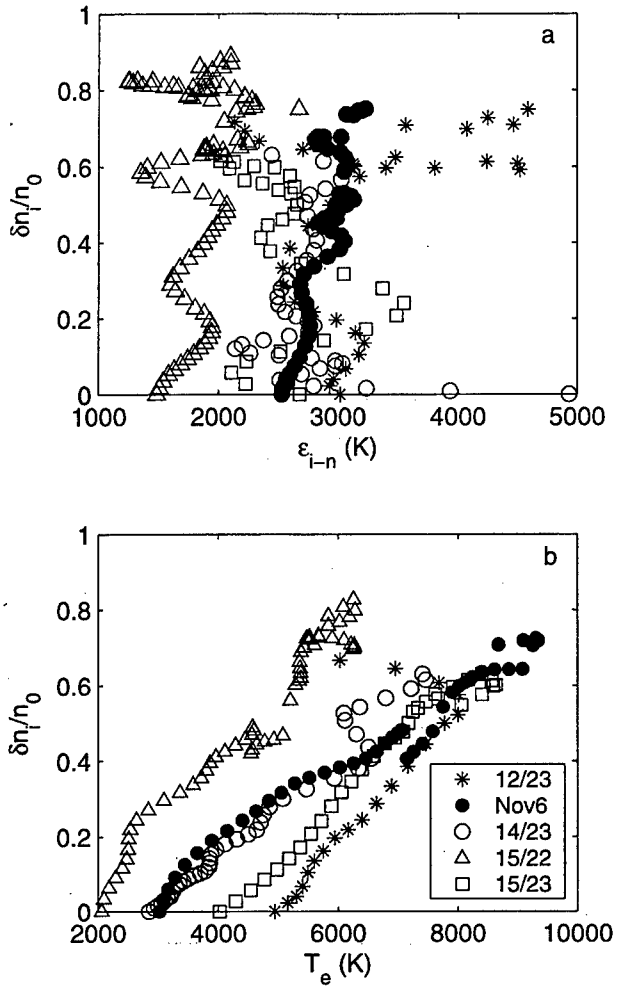

Figure 2. Variation of the relative plasma density (a) with the mean ion energy ε_{i-n} and (b) with electron temperature in five events studied (see text).

$\widetilde{a} \simeq 1$ and 1.25 in the northern (events 15/22 and Nov 6) and southern (events 12/23, 14/23, 15/23) hemispheres, respectively. For the 12/23 event, this tendency is violated in the vicinity of the wave structure, consistent with a raise in ε_{i-n}.

3. Rate Coefficients of Ion-Molecule Reactions

[19] Variations of the rate coefficients k_1 and k_2 with the energies of interacting species have been studied in numerous laboratory experiments. Experiments in drift tubes specified the dependences of k_1 and k_2 on the ion translational energy ε_i at rotational/translational $T_{1,2}$ and vibrational $T_V^{(1,2)}$ temperatures of molecular gas ~300 K [e.g., *McFarland et al.*, 1973; *Albritton et al.*, 1977]. Experiments in a high-temperature flowing afterglow device (HTFA) allow studies of the rate coefficients k_1 and k_2 at thermal equilibrium $T_i = T_{1,2} = T_V^{(1,2)}$ [e.g., *Viggiano and Williams*, 2001]. Analytical approximations for k_1 and k_2 derived from the recent HTFA experiments [*Hierl et al.*, 1997; *Viggiano and Williams*, 2001] are presented below. Hereafter, we use the normalized temperature $\tau_\xi = T_\xi[\mathrm{K}]/300$, where $\xi = i, e, n$, etc.

3.1. $O^+ + N_2$

[20] *Schmeltekopf et al.* [1967, 1968] determined specific rate coefficients $k_{1,V}$ for vibrational states of N_2 from $V = 0$ to 11 at $T_i = T_1 = 300$ K, that is $k_{1,V}/k_{1,0}|_{300\mathrm{K}} = c_V$. While $c_1 \simeq 1$, the rate coefficients for $V \geq 2$ increase dramatically; for example, $c_2 \simeq 38$, $c_3 \simeq 85$, $c_4 \simeq 220$, and $c_5 \simeq 270$. Comparing drift tube and HTFA data in the range of temperatures from 300 to 1800 K, *Hierl et al.* [1997] established that within the experimental uncertainty (~20%) the dependence on ε_i for vibrationally excited nitrogen is the same as for the ground state. Thus specific rate coefficients can be represented as $k_{1,V}(\varepsilon_i) = c_V \cdot k_{1,0}(\varepsilon_i)$. Correspondingly, k_1 is

$$k_1 \simeq k_{1,0}\left([N_2]^{(0)} + \sum_{V\geq 1} c_V \cdot [N_2]^{(V)}\right). \tag{4}$$

Here $[N_2]^{(V)}$ designates the population of the V vibrational state of N_2. An analytical approximation for $k_{1,0}$ was derived by *St.-Maurice and Torr* [1978] from the *Albritton et al.* [1977] drift tube data ($T_i = \frac{1}{3\kappa} m_i V_d^2$)

$$\begin{aligned} 10^{12} \cdot \widehat{k}_{1,0} &\simeq 1.5 - 0.6\tau_i + 0.09\tau_i^2 \qquad \text{at } 1 \leq \tau_i < 5.7 \\ &\simeq 2.7 - 1.15\tau_i + 0.15\tau_i^2 \qquad \text{at } 5.7 \leq \tau_i < 20. \end{aligned} \tag{5}$$

[21] Figure 3 shows the HTFA [*Hierl et al.*, 1997] (circles) and increased by 20% drift tube (squares) [*Albritton et al.*, 1977] data points along with $1.2 \cdot \widehat{k}_{1,0}$ (asterisks). Scaling compensates for small differences in the data sets that are well within the quoted error. The rate coefficient k_1 is

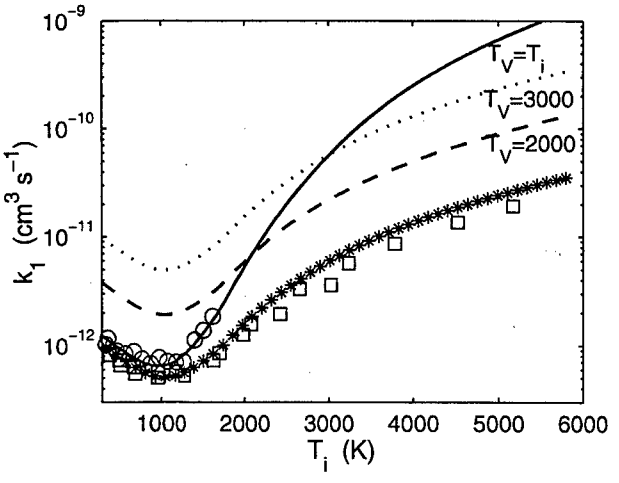

Figure 3. Rate coefficients for the reaction (R1). Circles and squares show the HTFA and increased by 20% drift tube data points, respectively; asterisks show $1.2 \cdot \widehat{k}_{1,0}$. Solid, dashed, and dotted lines show k_1 (equation (4)) calculated with $k_{1,0} = 1.2 \cdot \widehat{k}_{1,0}$ and with the Boltzmann distribution of $n_1^{(V)}$, assuming the vibrational temperature $T_V = T_i$, 2000, and 3000 K, respectively.

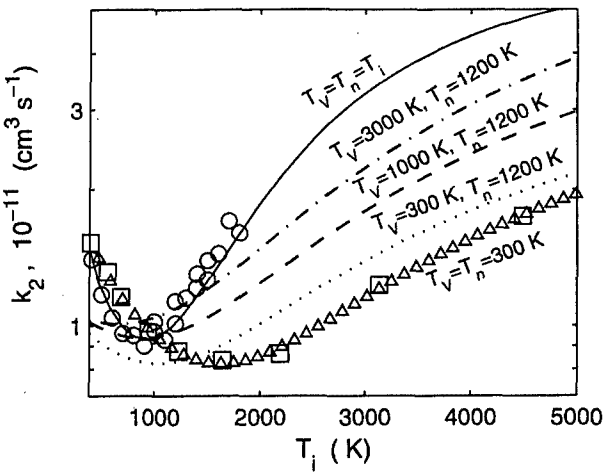

Figure 4. The rate coefficient for charge transfer (reaction (R2)). HTFA and (scaled) drift tube data points are shown by circles and squares, respectively. Triangles, dotted, dashed, dot-dashed, and solid lines show analytical approximations $10^{-11} \cdot k_{2,0}$ and k_2 for T_n = 1200 K and T_V = 300, 1000, and 3000 K, respectively.

calculated with $k_{1,0} \rightarrow 1.2 \cdot \widehat{k}_{1,0}$ and with the Boltzmann distribution of $[N_2]^{(V)}$. The calculation results are shown by solid, dashed, and dotted lines for vibrational temperatures $T_V^{(1)} = T_i$, 2000, and 3000 K, respectively. The analytical expression fits the experimental data extremely well [cf. *Pavlov*, 1998]. Note that the ground state rate coefficient $k_{1,0}$ increases rapidly only for large $T_i > 2000$ K, consistent with the event 12/23 in Figure 2a.

3.2. $O^+ + O_2$

[22] *Hierl et al.* [1997] also derived the dependence of k_2 on $T_V^{(2)}$. However, *Viggiano and Williams* [2001] showed that the contribution of the rotational temperature T_2 to the reaction rate is also significant. Plotted as functions of the total energy $\varepsilon_{tot} = 1.5T_i + T_2$, the HTFA [*Hierl et al.*, 1997] and drift tube [*McFarland et al.*, 1973] data points appear identical at small values of $\varepsilon_{tot} \leq 0.2$ eV (Figure 5 of *Viggiano and Williams* [2001]). Ascribing the difference between the two data sets at higher energies to the contribution of the first vibrational level [*Viggiano and Williams*, 2001] and assuming a Boltzmann distribution for the O_2 vibrational population $[O_2]^{(V)}$, one arrives at

$$k_2 \simeq 10^{-11} \cdot k_{2,0}\left\{[O_2]^{(0)} + [O_2]^{(1)}\left(\log_{10}\left(\tau_{\#}^{4.9}\right) - 2\right)\right\}$$
$$k_{2,0} \simeq \left(\frac{2.2}{(\tau_{\#} - 1)^{0.52}} + 6.05\exp\left(-\frac{34.04}{\tau_{\#} - 1}\right)\right) \quad (6)$$

($\tau_{\#} = 1.5\tau_i + \tau_n$). These approximations are shown in Figure 4 by triangles ($10^{-11} \cdot k_{2,0}$) and the solid line (k_2). Again, the analytical expression fits the experimental data well. Note that by virtue of the method of definition, the approximation in equation (6) is numerically close to that in Figure 3 [*Hierl et al.*, 1997] at $T_i \leq 1800$ K, lagging significantly behind at higher temperatures. We must now compare expectations for energy dependencies (equations (4) and (6)) with the experimental results in Figure 2.

4. Discussion

[23] Unlike E_0, the T_e enhancements within the SAPS rapidly decrease at altitudes below 300 km [e.g., *Newton and Walker*, 1975; *Foster et al.*, 1994]. Vibrational excitation due to electron impact depends strongly on T_e (see Figure 5). Furthermore, the number of "vibrationally active" electrons in the high-energy tail of the distribution decreases when the ratio $n_e/[N_2]$ falls below $\sim 10^{-3}$ [*Mishin et al.*, 2000]. Thus we anticipate little contribution from the vibrational mechanism at altitudes below ~300 km. Consequently, plasma density profiles caused by the vibrational mechanism should differ from those caused by strong electric fields. In particular, we expect a flat density altitude profile in the trough, similar to that found in Figure 6c of *Foster et al.* [1994].

[24] *Schunk et al.* [1975] stated that $T_V \simeq 4600$ K produces the same density profile as the electric field ~0.1 V/m or, equivalently, $T_{in} \simeq 4300$ K. Indeed, using the *Schmeltekopf et al.* [1968] specific rate coefficients that were scaled to rates at 300 K (see section 3.1), one gets that at $T_V \simeq 4600$ K the charge transfer rate $\simeq \widehat{k}_{1,0}(T_{in} = 4300) \simeq 10 \cdot \widehat{k}_{1,0}(T_{in} = 2000)$. Using the updated rate coefficients from Figure 3, one obtains $k_1(T_{in} = 2000, T_V = 3000) \simeq \widehat{k}_{1,0}(T_{in} = 4300)$. This means that the required level of vibrational excitations is significantly lowered. This, for example, may explain differences between the results of *Newton and Walker* [1975] and *Pavlov and Foster* [2001].

[25] Trough depths in the topside ionosphere are sometimes significantly smaller than those near the F peak [e.g., *Anderson et al.*, 1991]. However, they are sometimes comparable. For example, one can evaluate from Figure 6c [*Foster et al.*, 1994] that $\delta n_m \simeq 0.85$, 0.94, and 0.78 at altitudes 800, 400 (F peak), and 300 km, respectively. We do not have access to plasma parameters near the F peak during the topside ionosphere events studied here. On 6 November 2001 at ~0424 UT, the CHAMP satellite [*Riegber et al.*, 2002] (available at http://op.gfz-potsdam.de/champ/) detected $T_e = 4800$ K and $\delta n_m \simeq 0.7$ at ~450 km in the southern hemisphere. This event was simultaneous with, and magnetically conjugate to, the strong wave-structure event from DMSP F15 [*Mishin et al.*, 2003]. The density/temperature values in the topside ionosphere and

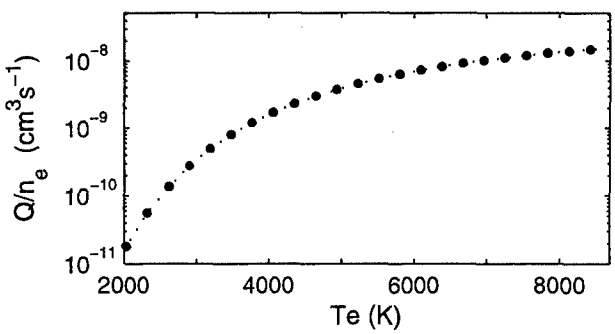

Figure 5. Rate coefficient for the vibrational excitation ($V = 0 \rightarrow V > 0$) of N_2 by thermal electrons.

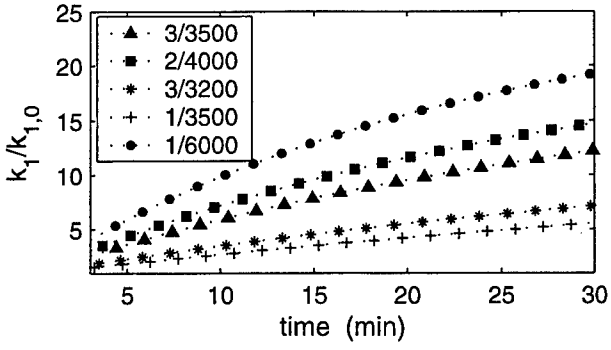

Figure 6. Variation of the $k_1/k_{1,0}$-ratio with time calculated at T_i = 2000 K with various combinations between $T_e \approx$ 3200, 3500, 4000, or 6000 K and n_e = (1, 2, or 3) × 10^5 cm^{-3}, designated in label: 3/3500 stands for n_e = 3 × 10^5 and T_e = 3500 K, et cetera.

near the magnetically conjugate *F* peak are close to those observed during the 21 March 1990 event by the Active satellite and Millstone Hill radar [*Förster et al.*, 1999].

[26] To evaluate ionization balance at altitudes at and below 400 km, one can use the local approximation [e.g., *Schunk et al.*, 1975]. Further, from Figures 3 and 4 it is clear that at $T_i \geq$ 2000 K the effects of vibrational excitations are more significant for k_1. Since $[N_2]/[O_2] \gtrsim 10$ in the topside ionosphere [e.g., *Hedin*, 1991], to first order one needs only to account for reaction (R1) at $T_V \geq$ 2000 K. The increase in the vibrational population of N_2 can be evaluated from

$$\frac{\partial}{\partial t}\eta_V \simeq \beta_V Q_V \eta_0 - L_V \eta_V + L_O \eta_{V+1}. \qquad (7)$$

Here Q_V and L_V are the production and loss rates of vibrational levels $\eta_V = [N_2]^{(V)}/[N_2]$, respectively. The total rate Q of vibrational excitation by (Maxwellian) thermal electrons is calculated using the cross sections from *Majeed and Strickland* [1997]. Figure 5 shows the dependence of Q/n_e on the electron temperature. The branching ratios for V = 1, 2, 3, and 4 at $T_e \geq$ 0.3 eV can be estimated as $\beta_V \sim$ 0.6, 0.3, 0.1, and 0.05, respectively. The contributions of suprathermal electrons via electronic triplet states and of transport processes are neglected. At altitudes ≥300 km the main quencher of vibrational states is atomic oxygen with the rate coefficient [*McNeal et al.*, 1974] $L_O \simeq 10^{-10} \cdot \exp(-70/T_n^{1/3}) \cdot [O]$ s^{-1} ([*O*] represents the atomic oxygen density). Accounting for charge transfer yields $L_V = L_O + c_V \cdot k_{1,0} \cdot n_i$ s^{-1}.

[27] The vibrational distribution is far from equilibrium, as $V - V$ exchange $\sim 5\ 10^{-13} \cdot [N_2]$ s^{-1} is insignificant at altitudes >300 km. To evaluate the charge exchange rate k_1, the population of the first five states ($\sum_0^5 \eta_V = 1$) was found, assuming $\eta_{V \geq 5} = 0$. Figure 6 shows $k_1/k_{1,0}$ versus time, calculated at T_i = 2000 K with various combinations between $T_e \approx$ 3200, 3500, 4000, or 6000 K and n_e = (1, 2, or 3) × 10^5 cm^{-3}.

[28] After ~5–10 min the production of NO^+ due to reaction (R1) intensifies. The recombination rate of NO^+ ions is ≲ 1/min for $n_e \geq 10^5$ cm^{-3}. Thus the density decay rate is of order $t_d^{-1} \simeq k_1 \cdot [N_2] \gtrsim 0.1$ min^{-1}. As the excitation rate $Q_V \propto n_e$, the density drop affects the variation of η_V and hence must be accounted for. To first order, the ionization balance can be described by reaction (R1) and

$$\frac{\partial}{\partial t} n_e = k_1(0)\, n_i(0)\, [N_2] - \alpha_r\, (n_e - n_i)\, n_e, \qquad (8)$$

assuming $n_e = n_i + [NO^+]$ and $n_i(0) = n_e(0)$; the recombination rate coefficient $\alpha_r \simeq 4 \times 10^{-7} \tau_e^{-0.5}$ cm^{-3} s^{-1}.

[29] Figure 7 shows the plasma density decrease in vibrationally excited gas. This was calculated with T_{in} = 2000 (dotted lines), 2500 (dashed lines), 3000 (dash-dotted lines), and 3500 K (solid lines) for T_e = 3500 and 4000 K and for the MSIS parameters of neutral gas at ~300 and 400 km, respectively. Apparently, within the decay time $\sim t_d$ the plasma density decreases by a factor of ~6 to ~10, that is $\delta n_i \simeq 0.8$–0.9.

[30] Figure 8 (top) shows the variation of the plasma density at ~300 km with time for T_{in} = 2000 K and T_e = 2000–5000 K. The relative plasma density at the end of run versus T_e is plotted in the bottom panel. The depth of the density depletion clearly increases with T_e. Note that the decay time is shorter, and the depletion is deeper at larger T_{in}, consistent with the results of *Schunk et al.* [1975].

[31] The decay time increases and the local approximation breaks in the topside ionosphere above ~500 km. To compare the modeling results with the DMSP observations at ~840 km, magnetic field-aligned transport processes (ambipolar diffusion) must be included. However, steady-state topside density profiles can be evaluated assuming diffusive equilibrium in a given temperature profile [cf. *Schunk et al.*, 1975]. The O^+ scale height is $H(O^+) \simeq \kappa(T_e + T_i)/(m_i g_\parallel)$, where $g_\parallel$ is the field-aligned component of gravitational acceleration. *Schunk et al.* [1975] obtained $H(O^+) \sim$ 300–350 km due to the large $T_i \propto E_0^2$. In the

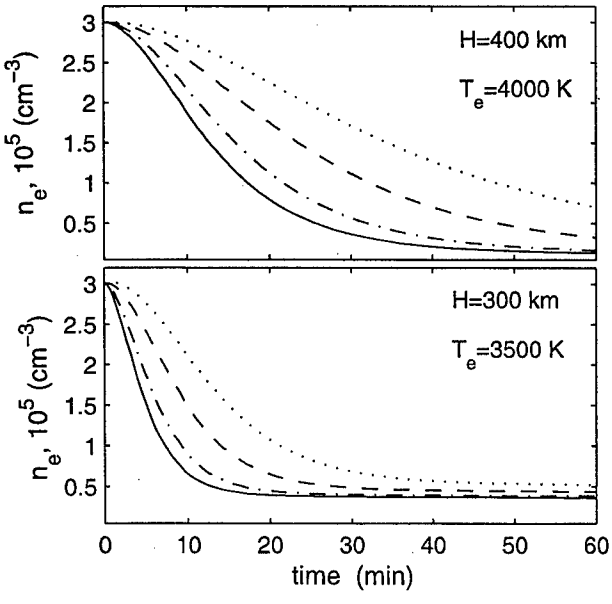

Figure 7. Density depletion at ~300 (bottom) and 400 km (top): T_{in} = 2000 (dotted lines), 2500 (dashed lines), 3000 (dash-dotted lines), and 3500 K (solid lines).

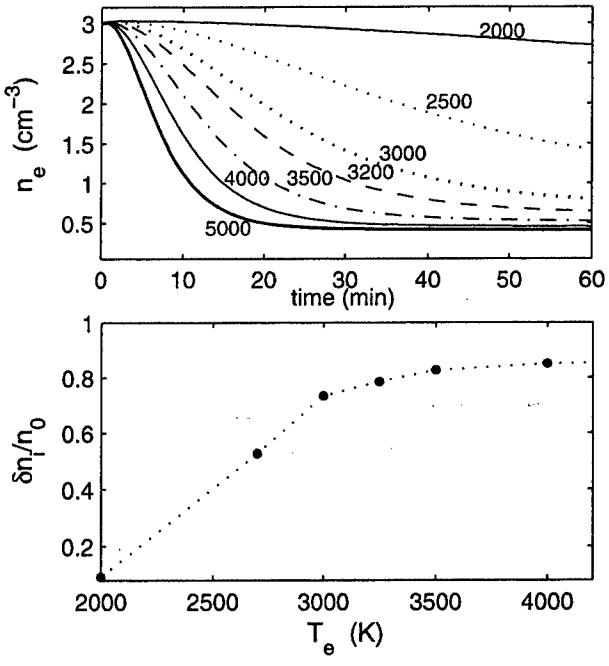

Figure 8. (top) Variation of the plasma density with time at 300 km for $T_e = 2000, \ldots 5000$ K; $T_{in} = 2000$ K. (bottom) Variation of the relative plasma density at the end of run with T_e.

events under consideration, even larger values of $H(O^+) \sim 400-500$ km are achieved due to elevated T_e.

[32] Thus nearly constant density versus height profiles should be established, yielding large δn_m from the bottom to the top of the trough [cf. *Foster et al.*, 1994]. Given that in the events under study, T_e at ~800 km is about twice as large as that at ~300–400 km, one can compare the topside observations (Figure 8) to the F peak modeling (Figure 2b). Good apparent agreement between them indicates that the vibrational mechanism is capable of forming deep density troughs or at the very least is a major contributor.

[33] One can outline the dynamics of the depletion process, as follows (no horizontal transport is involved). As soon as the F peak density decreases, the initial diffusive equilibrium breaks down. Plasma in the vicinity of the F peak flows into the density hole to restore the force balance along the flux tube. The plasma response resembles a rarefaction wave propagating from the F peak and can be described in terms of field-aligned ambipolar diffusion. The propagation time in the topside ionosphere is of the order of several $t_s \sim H(O^+)/v_s$, where $v_s \sim \sqrt{\kappa(T_e + T_i)/m_i}$. For the above parameters, one gets $t_s \sim 5-10$ min. As the F peak density decay rate $t_d^{-1} \gtrsim 0.1$ min^{-1} increases with n_e, "fresh" plasma increases the "processing" rate upon arrival.

[34] The depletion of a whole magnetic tube ends when the rates of plasma field-aligned transport in the topside ionosphere and decay in the depleted F peak match. This is achieved when the plasma density drops to several 10^4 cm^{-3} and the density gradient scale height becomes ~500 km. The time during which trough plasma achieves the steady state is of the order of several tens of minutes. This scenario, as depicted in Figure 9, predicts downward topside plasma flows within the trough, consistent with the observations.

[35] Two final remarks are in order. First, deexcitation of excited states, which might become important at high T_V, was not included in equation (7). This should slow down the process at low $T_e \leq 3000$ K, shifting the beginning of the saturation in Figure 8 (bottom) to somewhat higher temperatures. Second, for a given electron heating source, lower electron densities lead to higher electron temperatures. Thus the thermal energy balance equation must be included. Such modeling is well beyond the scope of this observation-based study.

5. Conclusion

[36] We report on subauroral plasma density troughs associated with the strong SAPS wave structure events observed by DMSP satellites during the major magnetic storm of 6 April 2000. The troughs were embedded within strongly irregular ≥500-km wide subauroral convection streams, composed of two distinctive parts. The poleward part coincided with the strong wave structure, energetic (ring current) ion precipitations, and enhanced vertical ion flows. One or several narrow density depletions were present here. The equatorward region was marked by a density trough coincident with a local maximum of the electron temperature ~7000–9000 K. Here the ion temperatures and downward vertical ion velocities were ~2000 K and ≲20 m/s, respectively. The mean horizontal convection velocity was typically ≲500 m/s.

[37] Analytical approximations for the rate coefficients of charge exchange reactions, derived from the latest labora-

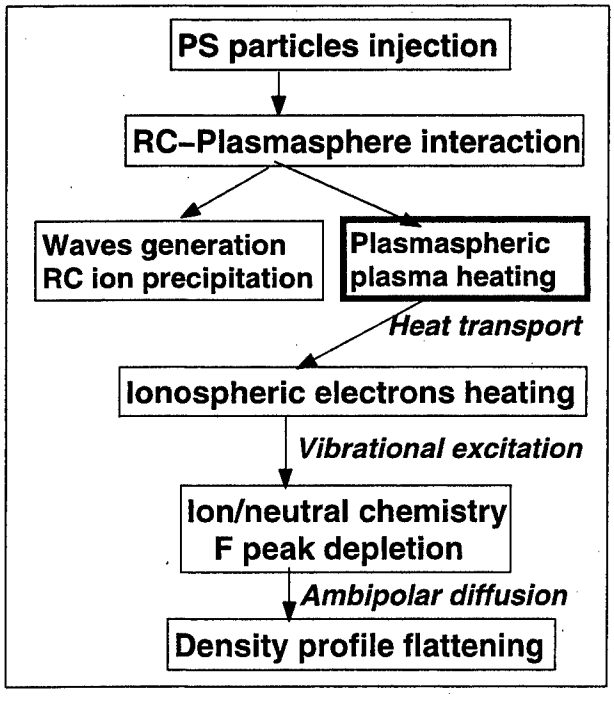

Figure 9. Block-diagram showing a scenario of the formation of the high-T_e related density trough (PS stands for plasma sheet).

tory experiments, were used for local modeling of the F peak density depletions in the equatorward regions. The topside density profiles were evaluated assuming diffusive equilibrium in a given T_e profile. Substantial apparent agreement with the observations indicates that the vibrational mechanism significantly contributes to the formation of the deep density troughs.

[38] **Acknowledgments.** We thank Fred Rich for help with DMSP data processing and discussions and David Cooke and Christopher Roth for providing the CHAMP satellite data. AE and SYMH indices were obtained through the website of the World Data Center for Geomagnetism, Kyoto. Some of the DMSP thermal plasma data were obtained through the DMSP SSIES data distribution website at the Center for Space Sciences of the University of Texas, Dallas. This research was supported in part by AFRL contract F19628-02-C-0012 with Boston College and by Air Force Office of Scientific Research under tasks 2311AS and 2303EP4.

[39] Arthur Richmond thanks Phillip Anderson and Matthias Foerster for their assistance in evaluating this paper.

References

Albritton, D., I. Dotan, W. Lindinger, M. McFarland, J. Tellinguisen, and F. Fehsenfeld (1977), Effects of ion speed distributions in flow-drift tube studies of ion-neutral reactions, *J. Chem. Phys.*, *66*, 410.

Anderson, P., R. Heelis, and W. Hanson (1991), The ionospheric signatures of rapid subauroral ion drifts, *J. Geophys. Res.*, *96*, 5785.

Anderson, P., W. Hanson, R. Hellis, J. D. Craven, D. Baker, and L. Frank (1993), A proposed production model of rapid subauroral ion drifts and their relationship to substorm evolution, *J. Geophys. Res.*, *98*, 6069.

Banks, P. M., and F. Yasuhara (1978), Electric fields and conductivity in the nighttime E region: A new magnetosphere-ionosphere-atmosphere coupling effect, *Geophys. Res. Lett.*, *5*, 1047.

Evans, J., J. Holt, W. Oliver, and R. Wand (1983), The fossil theory of nighttime high latitude F region troughs, *J. Geophys. Res.*, *88*, 7769.

Förster, M., J. Foster, J. Smilauer, K. Kudela, and A. Mikhailov (1999), Simultaneous measurements from the Millstone Hill radar and the Active satellite during the SAID/SAR arc event of the March 1990 CEDAR storm, *Ann. Geophys.*, *17*, 389.

Foster, J., and W. Burke (2002), A new categorization for subauroral electric fields, *Eos Trans. AGU*, *83*, 393.

Foster, J., M. Buonsanto, M. Mendillo, D. Nottingham, F. Rich, and W. Denig (1994), Coordinated stable auroral red arc observations: Relationship to plasma convection, *J. Geophys. Res.*, *99*, 11,429.

Galperin, Y., Y. Ponomarev, and A. Zosimova (1974), Plasma convection in the polar ionosphere, *Ann. Geophys.*, *30*, 1.

Garner, T., R. Wolf, R. Spiro, W. Burke, B. Fejer, S. Sazykin, J. Roeder, and M. Hairston (2004), Magnetospheric electric fields and plasma sheet injection to low L-shells during the 4–5 June 1991 magnetic storm: Comparison between the Rice Convection Model and observations, *J. Geophys. Res.*, *109*, A02214, doi:10.1029/2003JA010208.

Hardy, D. A., L. K. Schmidt, M. S. Gussenhoven, F. J. Marshall, H. C. Yeh, T. L. Shumaker, A. Huber, and J. Pantazis (1984), Precipitating electron and ion detectors (SSJ/4) for block 5D/Flights 4–10 DMSP satellites: Calibration and data presentation, *Tech. Rep. AFGL-TR-84-0317*, Air Force Geophys. Lab., Hanscom Air Force Base, Mass.

Hedin, A. (1991), Extension of the MSIS thermospheric model into the middle and lower atmosphere, *J. Geophys. Res.*, *96*, 1159.

Hierl, P., I. Dotan, J. Seeley, J. Van Doren, R. Morris, and A. Viggiano (1997), Rate constants for the reactions of O^+ with N_2 and O_2 as a function of temperature (300–1800 K), *J. Chem. Phys.*, *106*, 3540.

Huang, C. Y., and W. J. Burke (2004), Transient sheets of field-aligned currents observed by DMSP during the main phase of a magnetic superstorm, *J. Geophys. Res.*, *109*, A06303, doi:10.1029/2003JA010067.

Jordanova, V. K., R. Torbert, R. Thorne, H. Collin, J. Roeder, and J. Foster (1999), Ring current activity during the early $B_z < 0$ phase of the January 1997 magnetic cloud, *J. Geophys. Res.*, *104*, 24,895.

Kozyra, J., E. Shelley, R. Comfort, L. Brace, T. E. Cravens, and A. Nagy (1987), The role of ring current O^+ in the formation of stable auroral red arcs, *J. Geophys. Res.*, *92*, 7487.

Liemohn, M., J. Kozyra, P. Richards, G. Khazanov, M. Buonsanto, and V. Jordanova (2000), Ring current heating of the thermal electrons at solar maximum, *J. Geophys. Res.*, *105*, 27,767.

Majeed, T., and D. J. Strickland (1997), New survey of electron impact cross sections for photoelectron and auroral electron energy loss calculations, *J. Phys. Chem. Ref. Data*, *26*, 335.

McFarland, M., D. Albritton, F. Fehsenfeld, E. Ferguson, and A. Schmeltekopf (1973), Flow-drift technique for ion mobility and ion-molecule reaction rate constants measurements II. Positive ion reaction of N^+, O^+, and N_2^+ with O_2 and O^+ with N_2 from thermal to 2 eV, *J. Chem. Phys.*, *59*, 6620.

McNeal, R. J., M. Whitson, and G. Cook (1974), Temperature dependence of the quenching of vibrationally excifed nitrogen by atomic oxygen, *J. Geophys. Res.*, *79*, 1527.

Mishin, E., H. Carlson, and T. Hagfors (2000), On the electron distribution function in the F region and airglow enhancements during HF modification experiments, *Geophys. Res. Lett.*, *27*, 2857.

Mishin, E., W. Burke, C. Huang, and F. Rich (2003), Electromagnetic wave structures within subauroral polarization streams, *J. Geophys. Res.*, *108*(A8), 1309, doi:10.1029/2002JA009793.

Moffett, R., A. Ennis, G. Bailey, R. Heelis, and L. Brace (1998), Electron temperatures during rapid subauroral ion drift events, *Ann. Geophys.*, *16*, 450.

Newton, G., and J. Walker (1975), Electron density decrease in SAR arcs resulting from vibrationally excited nitrogen, *J. Geophys. Res.*, *80*, 1325.

Newton, G., J. Walker, and P. Meijer (1974), Vibrationally excited nitrogen in stable auroral red arcs and its effect on ionospheric recombination, *J. Geophys. Res.*, *79*, 3807.

Pavlov, A. (1998), The role of vibrationally excited oxygen and nitrogen in the ionosphere during the undisturbed and geomagnetic storm period of 6–12 April 1990, *Ann. Geophys.*, *16*, 589.

Pavlov, A., and J. Foster (2001), Model/data comparison of F region ionospheric perturbation over Millstone Hill during the severe geomagnetic storm of July 15–16, 2000, *J. Geophys. Res.*, *106*, 29,051.

Pavlov, A., T. Abe, and K.-I. Oyama (2000), Comparison of the measured and modeled electron densities and temperatures in the ionosphere and plasmasphere during 20–30 January, 1993, *Ann. Geophys.*, *18*, 1257.

Rees, M. H., and R. G. Roble (1975), Observations and theory of the formation of stable auroral red arcs, *Rev. Geophys.*, *13*, 201.

Reigber, C., H. Lühr, and P. Schwintzer (2002), CHAMP mission status, *Adv. Space Res.*, *30*(2), 129.

Rich, F. J., and M. Hairston (1994), Large-scale convection patterns observed by DMSP, *J. Geophys. Res.*, *99*, 3827.

Rich, F., P. Sultan, and W. Burke (2003), The 27-day variations of plasma densities and temperatures in the topside ionosphere, *J. Geophys. Res.*, *108*(A7), 1297, doi:10.1029/2002JA009731.

Schmeltekopf, A., F. Fehsenfeld, G. Gilman, and F. Ferguson (1967), Reaction of atomic oxygen ions with vibrationally excited nitrogen molecules, *Planet. Space Sci.*, *15*, 401.

Schmeltekopf, A., F. Ferguson, and F. Fehsenfeld (1968), Afterglow studies of the reactions He^+, He (2^3S), and NO with vibrationally excited N_2, *J. Chem. Phys.*, *48*, 2966.

Schunk, R., W. Raitt, and P. Banks (1975), Effect of electric fields on the daytime high-latitude E and F regions, *J. Geophys. Res.*, *80*, 3121.

Schunk, R., P. Banks, and W. Raitt (1976), Effect of electric fields and other processes upon the nighttime high-latitude F layer, *J. Geophys. Res.*, *81*, 3271.

Smith, P. H., and R. A. Hoffman (1974), Direct observations in the dusk hours of the characteristics of storm time ring current particles during the beginning of magnetic storms, *J. Geophys. Res.*, *79*, 964.

Spiro, R., R. Heelis, and W. Hanson (1979), Rapid subauroral ion drifts observed by Atmospheric Explorer C, *Geophys. Res. Lett.*, *6*, 657.

St.-Maurice, J.-P., and D. Torr (1978), Nonthermal rate coefficients in the ionosphere: The reactions of O^+ with N_2, O_2, and NO, *J. Geophys. Res.*, *83*, 969.

Viggiano, A., and S. Williams (2001), Ion-molecule kinetics at high temperatures (300–1800 K): Derivation of internal energy dependencies, *Adv. Gas Phase Ion Chem.*, *4*, 85.

Vlasov, M., and M. Kelley (2003), Modeling of the electron density depletion in the storm-time trough on April 20, 1985, *J. Atmos. Sol. Terr. Phys.*, *65*, 211.

W. J. Burke and A. A. Viggiano, Space Vehicles Directorate, Air Force Research Laboratory, Hanscom Air Force Base, MA 01731, USA. (william.burke2@hanscom.af.mil; albert.viggiano@hanscom.af.mil)

E. V. Mishin, Institute for Scientific Research, Boston College, 402 St Clements Hall, 140 Commonwealth Avenue, Chestnut Hill, MA 02467, USA. (evgenii.mishin@hanscom.af.mil)